

Autoionization-Enhanced Rydberg Dressing by Fast Contaminant Removal

Alec Cao[✉], Theodor Lukin Yelin[✉], William J. Eckner[✉], Nelson Darkwah Oppong[✉], and Adam M. Kaufman
*JILA, University of Colorado and National Institute of Standards and Technology, and Department of Physics,
 University of Colorado, Boulder, Colorado 80309, USA*

 (Received 14 October 2024; accepted 4 March 2025; published 31 March 2025)

Rydberg dressing is a powerful tool for entanglement generation in long-lived atomic states. While already employed effectively in several demonstrations, a key challenge for this technique is the collective loss triggered by blackbody-radiation-driven transitions to contaminant Rydberg states of opposite parity. We demonstrate the rapid removal of such contaminants using autoionization (AI) transitions found in alkaline-earth-like atoms. The AI is shown to be compatible with coherent operation of an array of optical clock qubits. By incorporating AI pulses into a stroboscopic Rydberg dressing (SRD) sequence, we enhance lifetimes by an order of magnitude for system sizes of up to 144 atoms, while maintaining an order of magnitude larger duty cycle than previously achieved. To highlight the utility of our approach, we use the AI-enhanced SRD protocol to improve the degree of achieved spin-squeezing during early time dressing dynamics. These results bring Rydberg dressing lifetimes closer to fundamental limits, opening the door to previously infeasible dressing proposals.

DOI: [10.1103/PhysRevLett.134.133201](https://doi.org/10.1103/PhysRevLett.134.133201)

Neutral atoms are a versatile platform for quantum science. A key tool of this platform is coupling to high-lying Rydberg states for access to strong interactions [1–3]. These interactions have featured prominently in recent advances for high-fidelity gates [4–8], quantum many-body simulation [9–14], and entanglement-enhanced metrology [15–20]. One coupling scheme which has garnered substantial theoretical interest is Rydberg dressing [21–38], in which a detuned laser causes the Rydberg van der Waals potential to be effectively experienced as a softcore interaction in a long-lived state [23,28]. In this way, dressing enables on-demand interactions in a high-coherence, controllable subspace. Experimentally, Rydberg dressing has been used to implement entangling gates [15,39], many-body spin dynamics [16,40–43], and extended Hubbard models [44,45].

A major limitation for Rydberg dressing is blackbody radiation (BBR) [46], which can trigger collective losses, as shown in Fig. 1(b). In this process, BBR drives transitions from the target Rydberg state $|r\rangle$ to a set of nearby, opposite-parity Rydberg (contaminant) states $|r'\rangle$. The resonant dipolar exchange interaction of $|r'\rangle$ with $|r\rangle$ [47,48] can shift the dressing laser into resonance, facilitating a proliferation of Rydberg excitations. Signatures of collective loss have been observed in a number of Rydberg dressing experiments [16,18,40,49,50], as well as in Rydberg spectra of Bose condensates [51–53]. Critically, the collective loss can be triggered by only a single contaminant (Rydberg atom), causing the loss rate to grow for increasing ensemble size.

Collective loss can be mitigated by applying the Rydberg laser in a series of short pulses with sufficiently long wait

times in between [52,53,64]. Contaminants created during each short pulse decay back to low-lying atomic states during the wait, preventing facilitated excitation on subsequent pulses. The suppression of collective loss in dressing was recently demonstrated using such a stroboscopic Rydberg dressing (SRD) protocol [18]. Compared to continuous Rydberg dressing (CRD) with a single pulse, this SRD strategy suffers from a low duty cycle [65] as a result of waiting for the contaminants to decay. A fast contaminant removal procedure can be used to overcome this limitation. In divalent atoms, such removal can be performed by exciting the remaining core electron to an autoionizing (AI) state [66,67]; from this state, the Rydberg electron is ejected due to its interaction with the core electron. Critically, both the core excitation and subsequent AI can occur orders of magnitude faster than typical contaminant state decay. Since the core transition frequency is relatively insensitive to the Rydberg state, a single AI laser is capable of removing all dominantly populated contaminant states, reducing experimental overhead. Previously, AI has been used for improved Rydberg detection schemes [68–72] and the core transition polarizability for shifting the Rydberg state energy [73,74].

In this Letter, we report on fast contaminant removal via AI in a Rydberg-dressed strontium atom array. We first show the compatibility of AI with coherent state manipulation, showing negligible impact on optical clock qubit coherence and further Rydberg excitation. We then integrate AI with SRD, achieving an order of magnitude suppression of collective loss for two-dimensional ensembles of up to 144 atoms; a Rydberg duty cycle near the 10% level is maintained, compared to $< 1\%$ realized previously

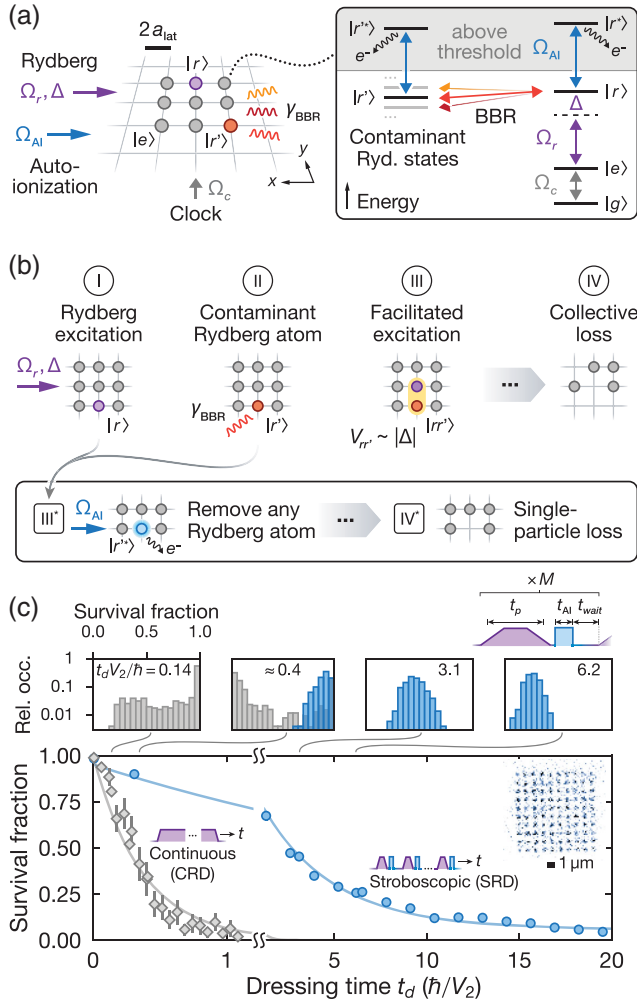


FIG. 1. Suppressing collective loss in Rydberg-dressed atom arrays. (a) Schematic illustration of the experimental setup with ^{88}Sr atoms (circles) trapped in an optical lattice (gray lines) and lasers (colored arrows) driving the clock, Rydberg, and AI transitions. BBR photons (γ_{BBR} , wiggly lines) couple the target Rydberg state $|r\rangle$ to contaminant states $|r'\rangle$. (right) Electronic states, transitions, and couplings relevant for Rydberg dressing and AI. (b) Collective-loss mechanism in Rydberg-dressed atom arrays separated into steps (I–IV) for visual clarity: BBR generates contaminant atoms $|r'\rangle$; this enables facilitated excitation and subsequent collective loss if the pair potential $V_{rr'} \sim |\Delta|$ matches the laser detuning Δ . (bottom, III and IV*) Removal of (contaminant) Rydberg atoms through AI suppresses the collective-loss mechanism. Ellipses (...) indicate omitted steps such as Rydberg-atom decay. (c) Survival of an $N_{\text{tot}} = 10 \times 10$ atom array after variable Rydberg dressing time t_d with CRD (gray diamonds) and SRD (blue circles). Solid lines are numerical fits [54]. Error bars are standard error of the mean and partly smaller than the marker size. Top right of main panel shows a single-shot fluorescence image. Upper histograms show the relative occurrence rate of observing different survival fractions at specific times, obtained from ≈ 500 independent repetitions of the experiment. Top right diagram shows pulse sequence for SRD.

without AI [18]. Finally, we explicitly demonstrate the utility of our approach by investigating spin squeezing [16,18,28]. In a regime with significant collective loss at the optimal squeezing time, we recover 3 dB of Wineland spin squeezing with AI-enhanced SRD while suppressing around 5 dB of noise relative to CRD. For the remainder of the text, we will refer to our AI-enhanced SRD protocol simply as SRD.

Our experiment, schematically illustrated in Fig. 1(a), consists of strontium optical clock qubits ($|g\rangle = 5s^21S_0$, $|e\rangle = 5s5p^3P_0$) in an optical lattice of spacing $a_{\text{lat}} \approx 575$ nm [16,19]. N_{tot} atoms are arranged into rectangular ensembles of dimension $L_x \times L_y \geq N_{\text{tot}}$, with a typical filling fraction of around 97% and $2a_{\text{lat}}$ or $3a_{\text{lat}}$ spacing. The clock state is coupled to the Rydberg state $|r\rangle = 5s47s^3S_1$. To suppress nonadiabatic Rydberg excitations, dressing pulses are performed by ramping up to and down from a Rabi frequency $\Omega_r = 2\pi \times 3$ MHz in $0.2 \mu\text{s}$; simultaneously, the detuning Δ is ramped between $4\Omega_r$ and $2\Omega_r$, yielding a maximum dressing parameter $\beta = \Omega_r/2\Delta = 0.25$. Conceptually, β characterizes the admixture of Rydberg character in the dressed state $|\tilde{e}\rangle \sim |e\rangle + \beta|r\rangle$ which $|e\rangle$ is adiabatically connected to. BBR primarily drives transitions from $|r\rangle$ to nearby contaminant states $|r'\rangle$ in the $5snp^3P_{0,1,2}$ Rydberg series. A $\lambda \approx 407.89$ nm AI laser [54] is used to excite the core electron to a $5p_{3/2}nl$ AI state; notationally, we distinguish between the $|r^*\rangle = 5p_{3/2}47s_{1/2}$ state excited from the target Rydberg state $|r\rangle$ and other $|r'^*\rangle$ states excited from all other BBR populated states $|r'\rangle$ [see Fig. 1(a) inset].

The core result of this Letter is shown in Fig. 1(c). The experiment starts by preparing a 10×10 atom array in the clock state $|e\rangle$. We probe the survival over time in $|e\rangle$ after Rydberg dressing for two protocols. For CRD, we apply a single ($M = 1$) dressing pulse while varying the pulse duration t_p . For SRD, we apply a variable number M of dressing pulses, each with a fixed $t_p \approx 0.23 \mu\text{s}$ [54]; in between dressing pulses, AI pulses of duration $t_{\text{AI}} = 0.3 \mu\text{s}$ are applied, followed by a wait time of $t_{\text{wait}} = 2 \mu\text{s}$. The total dressing time for both cases is defined as $t_d = Mt_p$. Dressing times are plotted with respect to the calculated two-body interaction energy $V_2 = \beta^3 \hbar \Omega_r (1 + 2N\beta^2)^{-3/2}/2$, with N the effective number of atoms in a Rydberg blockade radius [18,54]. The data show an order of magnitude improvement in the dressing lifetime for SRD over CRD. The survival histograms at specific times reveal the collective loss and its suppression by AI. For CRD, a low survival tail rapidly develops even at relatively short times, and ultimately the distribution becomes multimodal with peaks around full survival and full loss [40]. This structure can be understood intuitively from a quantum jump perspective, with the different peaks corresponding to whether or not a BBR-induced jump (and subsequent collective loss) occurred. In contrast, the SRD case shows

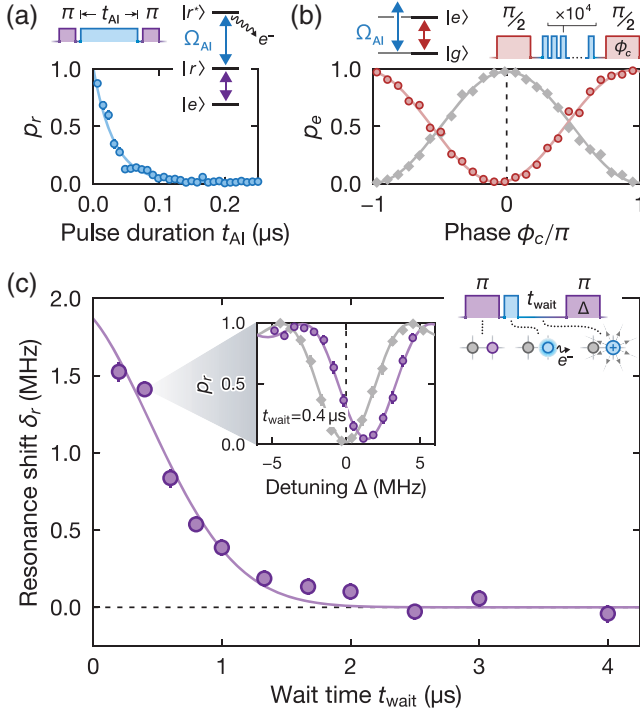


FIG. 2. Characterizing autoionization of $n = 47 \text{ } ^3\text{S}_1$ Rydberg atoms. (a) Duration of the AI process obtained by applying the AI laser for variable duration t_{AI} . Here, p_r (blue circles) corresponds to the detection probability in $|r\rangle$. (b) Stark shift of the AI laser on the optical clock transition. Ramsey fringe (red circles) after application of 10^4 $t_{\text{AI}} = 0.2 \text{ } \mu\text{s}$ -long AI pulses during the dark time. Gray diamonds correspond to a reference measurement without the AI laser. The fitted fringe contrast is $C = 0.977(4)$ [0.970(4)] with [without] applying the AI pulses and p_e corresponds to the detection probability in $|e\rangle$. (c) Transient Rydberg resonance shift (purple circles) for variable wait time t_{wait} after applying a $t_{\text{AI}} = 0.3 \text{ } \mu\text{s}$ AI pulse to a nearby Rydberg atom (initial separation $d = 3a_{\text{lat}}$), as illustrated in the top right schematic. Purple circles in the inset show an example spectroscopy measurement at $t_{\text{wait}} = 0.4 \text{ } \mu\text{s}$. Gray diamonds show a reference spectroscopy measurement. In panels (a)–(c), pulse diagrams illustrate the experimental sequence with all atoms starting in $|e\rangle$ for (a),(c) and $|g\rangle$ for (b). Solid lines are numerical fits, and error bars indicate Clopper-Pearson confidence intervals for probabilities p and fit errors for δ .

a unimodal distribution which steadily decays. By quickly removing the BBR-induced contaminants with AI, facilitated excitation is never triggered, and essentially single-particle loss is recovered.

To determine the potential improvement in SRD duty cycle, we characterize the AI rate in Fig. 2(a) by measuring the survival of atoms prepared in $|r\rangle$ after an AI pulse of duration t_{AI} . The data show a $1/e$ timescale of $\tau_{\text{AI}} = 31(2) \text{ ns}$, which is three orders of magnitude faster than the relevant Rydberg state lifetimes [19]. The rate is currently limited by the AI laser intensity which determines the Rabi frequency Ω_{AI} that the core transition $|r\rangle \leftrightarrow |r^*\rangle$ is driven at [54]; the fundamental limit of roughly

$\Gamma_{\text{AI}}^{-1} \approx 15 \text{ ps}$ is set by the intrinsic ionization rate Γ_{AI} of $|r^*\rangle$ [67,75]. The intrinsic rate varies with Rydberg principal number and angular momentum [66,76,77] but will be similar for the states $|r^*\rangle$ dominantly populated by BBR. To ensure a high degree of contaminant removal, we use $t_{\text{AI}} = 0.2\text{--}0.3 \text{ } \mu\text{s}$ for SRD.

The AI leaves behind an ion [78] which substantially alters the nearby electric field environment, disturbing subsequent Rydberg excitation. We investigate this effect in Fig. 2(c). Isolated atom pairs are prepared into the Bell state $(|er\rangle + |re\rangle)/\sqrt{2}$ by performing a blockaded π pulse [71,79]. After AI of the $|r\rangle$ state, we perform Rydberg spectroscopy on the remaining $|e\rangle$ atom. This atom samples the ion-generated field, shifting the resonance by δ_r (inset). We observe δ_r decay for longer durations t_{wait} after the AI pulse as the ion moves further away. The dominant mechanism for ejecting the ions is likely to be acceleration by stray electric fields, which we infer to be at the $360(20) \text{ mV/cm}$ level [54]. For use in Rydberg dressing, we fix $t_{\text{wait}} = 2 \text{ } \mu\text{s}$, which is the dominant limitation for the currently achievable duty cycle.

In Fig. 2(b), we further show that exposure to the AI laser does not substantially degrade optical-clock-qubit coherence. Employing a standard Ramsey interferometry protocol, we find that the fringe contrast is not reduced even after applying 10^4 AI pulses during the dark time. From a separate Ramsey measurement, we infer a differential clock-transition Stark shift of $235.6(1) \text{ Hz}$ due to the AI laser, consistent with expectation from the measured AI rate [54]. The phase shift per $1/e$ AI time, which is independent of AI laser intensity in the currently relevant regime $\Omega_{\text{AI}} \ll \Gamma_{\text{AI}}$, is $2\pi \times 7.3(5) \text{ } \mu\text{rad}$.

With the AI process well characterized, we now return to assessing the Rydberg dressing lifetime improvement using SRD. While more sophisticated modeling for collective loss dynamics has been developed [52,80], we choose to simply characterize the dressing lifetime by a $1/e$ decay time $\tau_{1/e}$ extracted from an empirical fit of the survival p_e over dressing time t_d [54]. We begin by investigating $\tau_{1/e}$ for SRD as a function of pulse duration t_p (with fixed ramp time) in Fig. 3(a). For these data, a 10×10 ensemble is initially prepared in the equal superposition $(|g\rangle + |e\rangle)/\sqrt{2}$ prior to dressing. The decay time shows a monotonic decrease for longer t_p as the per-pulse probability of BBR-induced decay and subsequent Rydberg facilitation is increased. For the remaining results, we set t_p to the lowest value shown, corresponding to an $\approx 8\%$ duty cycle for the largest systems explored.

To illustrate the suppression of the collective nature of the loss, we investigate $\tau_{1/e}$ as a function of density and system size in Figs. 3(b) and 3(c), respectively. As a proxy for density, we vary the average initial excitation fraction $\langle N_e \rangle / N_{\text{tot}} = \sin^2(\theta/2)$ by preparing each atom of a 10×10 array into the superposition $\cos(\theta/2)|g\rangle + \sin(\theta/2)|e\rangle$ with a clock θ pulse. To vary the system size, we instead use

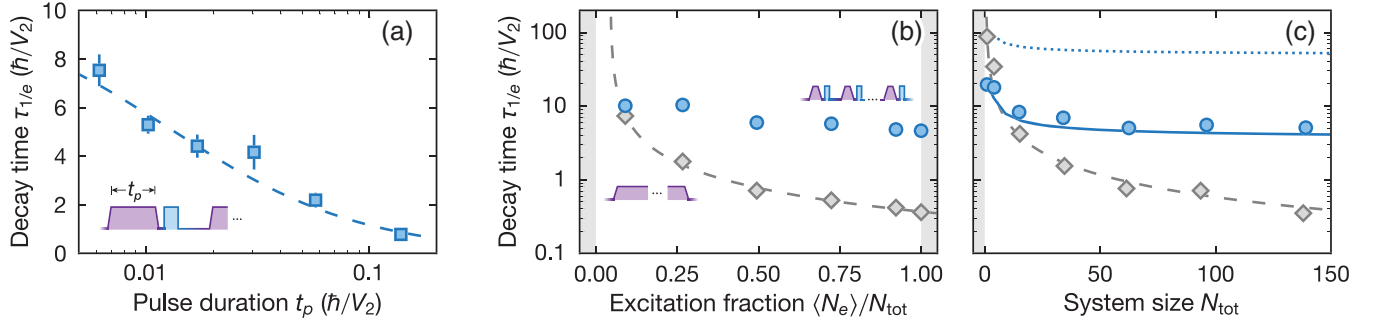


FIG. 3. Benchmarking contaminant removal through autoionization laser pulses. (a) Decay time $\tau_{1/e}$ (blue squares) for variable Rydberg dressing pulse duration t_p in the SRD protocol, as illustrated in the bottom left inset pulse diagram. (b),(c) Decay time $\tau_{1/e}$ for (b) variable initial excitation fraction $\langle N_e \rangle / N_{\text{tot}}$ in a constant $N_{\text{tot}} = 10 \times 10$ array and (c) variable system size $N_{\text{tot}} = \sqrt{N_{\text{tot}}} \times \sqrt{N_{\text{tot}}}$ at constant $\langle N_e \rangle / N_{\text{tot}} = 1/2$. Blue circles (gray diamonds) correspond to SRD (CRD) protocols [see inset pulse diagrams in panel (b)]. Gray shaded regions indicate (experimentally) inaccessible regions. In panel (c), the solid blue line shows a constant $\tau_{1/e}(N_{\text{tot}} = 1)$ [i.e., only scaled by the variation in $V_2(N_{\text{tot}})$], and the dotted blue line shows the ideal Rydberg-decay-limited dressing lifetime. In all panels, dashed lines indicate numerical fits of $\tau_{1/e}^{-1}$ to a linear form. Each data point is extracted from a numerical fit and error bars indicate bootstrapped fit errors (partly smaller than marker size).

arrays of variable size $N_{\text{tot}} = \sqrt{N_{\text{tot}}} \times \sqrt{N_{\text{tot}}}$ with fixed $\theta = \pi/2$ ($\langle N_e \rangle / N_{\text{tot}} = 1/2$). Indeed, we observe a markedly steeper decrease of the decay time with both excitation fraction and system size for CRD compared to SRD. For the largest and densest systems, the lifetime improvement using SRD is an order of magnitude.

The SRD results are not yet at the fundamental limit τ_r/p_r set by the Rydberg state lifetime τ_r and dressing fraction p_r [Fig. 3(c) dotted line]. One challenge is non-adiabaticity of the pulses. Indeed the faster single-atom ($N_{\text{tot}} = 1$) decay for SRD compared to CRD appears to be explained by nonadiabaticity based on numerical simulations [54]. Interestingly, we find that the trend in $\tau_{1/e}$ with larger N_{tot} for SRD is roughly consistent with just the variation in V_2 at a fixed per-atom loss rate (solid line). The degree to which nonadiabatic excitations affect $\tau_{1/e}$ for these larger systems is less clear, but nonadiabaticity certainly limits the minimum pulse duration which sets the residual collective loss within a single pulse [Fig. 3(a)]. Further improving the dressing lifetime remains an open challenge; nevertheless, the current results already demonstrate qualitatively improved scaling of dressing lifetimes for large systems by using SRD.

To explicitly demonstrate the utility of our approach, we investigate spin squeezing using SRD in Fig. 4. Compared to an unentangled coherent spin state (CSS), spin-squeezed states feature reduced projection noise along a given spin quadrature to achieve quantum-enhanced measurement precision [81,82]. Spin squeezing is naturally generated by the soft-core Ising interactions of Rydberg dressing [16,18,28], which implement a finite-range version of the canonical one-axis twisting Hamiltonian [83]. The spin-squeezing protocol is shown in the diagram of Fig. 4(a), following the procedure in Ref. [16]. We measure the differential observable $d_z = S_z^A / N_{\text{tot}}^A - S_z^B / N_{\text{tot}}^B$ between a pair (A, B) of 5×14 ensembles to reject technical noise.

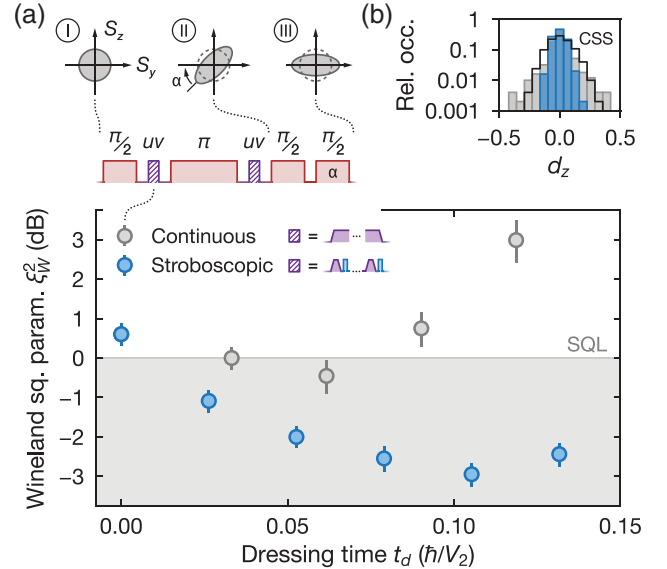


FIG. 4. Preparing spin-squeezed states with autoionization-enhanced stroboscopic Rydberg dressing. (a) (top) Pulse sequence for the preparation of spin-squeezed states and schematic illustration of the quasi-probability on the Bloch sphere (2D projection shown) at different points (I)–(III) in the sequence. The pulses labelled “uv” correspond to either CRD or SRD (see legend). (bottom) Wineland squeezing parameter ξ_W^2 determined from variance and contrast measurements at variable dressing time t_d for CRD (gray circles) and SRD (blue circles). Here, ξ_W^2 is determined from a differential measurement between two independent ensembles each with $N_{\text{tot}} \approx 68$ atoms. Note that the $t_d = 0$ data corresponds to an unentangled CSS. SQL denotes the standard quantum limit. (b) Histogram of the differential observable d_z obtained for the variance measurements in panel (a) at $t_d \approx 0.11\hbar/V_2$ for SRD (blue) and $t_d \approx 0.12\hbar/V_2$ for CRD (gray). Black lines correspond to a reference measurement with a CSS.

The measured distribution of d_z after a dressing time $t_d \approx 0.11\hbar/V_2$ is shown in Fig. 4(b). While collective loss leads to wide wings for CRD, the SRD shows a distribution which is strictly more narrow than the CSS ($t_d = 0$). The metrological gain can be characterized by the Wineland squeezing parameter ξ_{W}^2 [81,82], which accounts for both the variance in d_z as well as the spin vector length which we extract from a Ramsey fringe. The improved gain is shown in the bottom panel of Fig. 4(a) where the SRD achieves around 3 dB below the standard quantum limit (SQL). In contrast, the squeezing begins to degrade much earlier for CRD as the collective loss sets in, limiting the improvement to < 1 dB. We note that the CRD results are significantly worse than realized in our previous work [16]. We are currently investigating the source of this discrepancy, but we emphasize that it is unlikely to be related to AI, which is not used for CRD; given this and the near-SQL performance of the CSS, we suspect the disparity is related to the Rydberg laser.

In conclusion, we have demonstrated the use of AI for enhanced Rydberg dressing. By removing BBR-generated contaminants using AI in a SRD protocol, we achieved a tenfold improvement in dressing lifetime for 144-atom systems while maintaining an order of magnitude larger duty cycle than previous work without AI [18]. We showed that SRD is compatible with coherent operation of an optical clock qubit, and demonstrated improved spin squeezing at short dressing times. The duty cycle could be further improved by incorporating fast-switching electrodes [84] for rapid ion removal and increasing the AI laser intensity. The extended lifetimes of our protocol open the door to longer-time, larger-scale quantum simulations of spin models, which can, for instance, enable improved spin squeezing [36,38] or exploration of exotic many-body physics [26,31,33]. Alternatively, direct detection of the ionized contaminants could be a useful tool in erasure conversion schemes [5,13,85].

Acknowledgments—We acknowledge J. Ye and his lab for the operation and provision of the silicon-crystalline-cavity-stabilized clock laser. We acknowledge stimulating discussions with S. Hollerith, W.R. Milner, R. Potvliege, P. Weckesser, J. T. Young, J. Zeiher. The authors also wish to thank A. Carroll and R. Kaubruegger for careful readings of the manuscript and helpful comments. This material is based upon work supported by the Army Research Office (W911NF-22-1-0104), the National Science Foundation QLCI (OMA-2016244), the National Science Foundation JILA-Physics Frontier Center (PHY-2317149), the U.S. Department of Energy, Office of Science, the National Quantum Information Science Research Centers, Quantum Systems Accelerator, and the National Institute of Standards and Technology. We also acknowledge funding from Lockheed Martin. A.C. acknowledges support from the NSF Graduate Research Fellowship

Program (Grant No. DGE2040434); W. J. E. acknowledges support from the NDSEG Fellowship; N. D. O. acknowledges support from the Alexander von Humboldt Foundation.

-
- [1] M. Saffman, T. G. Walker, and K. Mølmer, Quantum information with Rydberg atoms, *Rev. Mod. Phys.* **82**, 2313 (2010).
 - [2] A. Browaeys and T. Lahaye, Many-body physics with individually controlled Rydberg atoms, *Nat. Phys.* **16**, 132 (2020).
 - [3] M. Morgado and S. Whitlock, Quantum simulation and computing with Rydberg-interacting qubits, *AVS Quantum Sci.* **3**, 023501 (2021).
 - [4] S. J. Evered, D. Bluvstein, M. Kalinowski, S. Ebadi, T. Manovitz, H. Zhou, S. H. Li, A. A. Geim, T. T. Wang, N. Maskara *et al.*, High-fidelity parallel entangling gates on a neutral atom quantum computer, *Nature (London)* **622**, 268 (2023).
 - [5] S. Ma, G. Liu, P. Peng, B. Zhang, S. Jandura, J. Claes, A. P. Burgers, G. Pupillo, S. Puri, and J. D. Thompson, High-fidelity gates with mid-circuit erasure conversion in a metastable neutral atom qubit, *Nature (London)* **622**, 279 (2023).
 - [6] M. Peper, Y. Li, D. Y. Knapp, M. Bileska, S. Ma, G. Liu, P. Peng, B. Zhang, S. P. Horvath, A. P. Burgers, and J. D. Thompson, Spectroscopy and modeling of ^{171}Yb Rydberg states for high-fidelity two-qubit gates, *Phys. Rev. X* **15**, 011009 (2025).
 - [7] R. B.-S. Tsai, X. Sun, A. L. Shaw, R. Finkelstein, and M. Endres, Benchmarking and fidelity response theory of high-fidelity Rydberg entangling gates, *PRX Quantum* **6**, 010331 (2025).
 - [8] A. G. Radnaev, W. C. Chung, D. C. Cole, D. Mason, T. G. Ballance, M. J. Bedalov, D. A. Belknap, M. R. Berman, M. Blakely, I. L. Bloomfield *et al.*, A universal neutral-atom quantum computer with individual optical addressing and non-destructive readout, [arXiv:2408.08288](https://arxiv.org/abs/2408.08288).
 - [9] S. Ebadi, T. T. Wang, H. Levine, A. Keesling, G. Semeghini, A. Omran, D. Bluvstein, R. Samajdar, H. Pichler, W. W. Ho *et al.*, Quantum phases of matter on a 256-atom programmable quantum simulator, *Nature (London)* **595**, 227 (2021).
 - [10] P. Scholl, M. Schuler, H. J. Williams, A. A. Eberharter, D. Barredo, K.-N. Schymik, V. Lienhard, L.-P. Henry, T. C. Lang, T. Lahaye, A. M. Läuchli, and A. Browaeys, Quantum simulation of 2D antiferromagnets with hundreds of Rydberg atoms, *Nature (London)* **595**, 233 (2021).
 - [11] G. Semeghini, H. Levine, A. Keesling, S. Ebadi, T. T. Wang, D. Bluvstein, R. Verresen, H. Pichler, M. Kalinowski, R. Samajdar *et al.*, Probing topological spin liquids on a programmable quantum simulator, *Science* **374**, 1242 (2021).
 - [12] C. Chen, G. Bornet, M. Bintz, G. Emperauger, L. Leclerc, V. S. Liu, P. Scholl, D. Barredo, J. Hauschild, S. Chatterjee *et al.*, Continuous symmetry breaking in a two-dimensional Rydberg array, *Nature (London)* **616**, 691 (2023).
 - [13] P. Scholl, A. L. Shaw, R. B.-S. Tsai, R. Finkelstein, J. Choi, and M. Endres, Erasure conversion in a high-fidelity

- Rydberg quantum simulator, *Nature (London)* **622**, 273 (2023).
- [14] A. L. Shaw, Z. Chen, J. Choi, D. K. Mark, P. Scholl, R. Finkelstein, A. Elben, S. Choi, and M. Endres, Benchmarking highly entangled states on a 60-atom analogue quantum simulator, *Nature (London)* **628**, 71 (2024).
- [15] N. Schine, A. W. Young, W. J. Eckner, M. J. Martin, and A. M. Kaufman, Long-lived Bell states in an array of optical clock qubits, *Nat. Phys.* **18**, 1067 (2022).
- [16] W. J. Eckner, N. Darkwah Oppong, A. Cao, A. W. Young, W. R. Milner, J. M. Robinson, J. Ye, and A. M. Kaufman, Realizing spin squeezing with Rydberg interactions in an optical clock, *Nature (London)* **621**, 734 (2023).
- [17] G. Bornet, G. Emperauger, C. Chen, B. Ye, M. Block, M. Bintz, J. A. Boyd, D. Barredo, T. Comparin, F. Mezzacapo *et al.*, Scalable spin squeezing in a dipolar Rydberg atom array, *Nature (London)* **621**, 728 (2023).
- [18] J. A. Hines, S. V. Rajagopal, G. L. Moreau, M. D. Wahrman, N. A. Lewis, O. Marković, and M. Schleier-Smith, Spin squeezing by Rydberg dressing in an array of atomic ensembles, *Phys. Rev. Lett.* **131**, 063401 (2023).
- [19] A. Cao, W. J. Eckner, T. Lukin Yelin, A. W. Young, S. Jandura, L. Yan, K. Kim, G. Pupillo, J. Ye, N. Darkwah Oppong, and A. M. Kaufman, Multi-qubit gates and Schrödinger cat states in an optical clock, *Nature (London)* **634**, 315 (2024).
- [20] R. Finkelstein, R. B.-S. Tsai, X. Sun, P. Scholl, S. Direkci, T. Gefen, J. Choi, A. L. Shaw, and M. Endres, Universal quantum operations and ancilla-based read-out for tweezer clocks, *Nature (London)* **634**, 321 (2024).
- [21] I. Bouchoule and K. Mølmer, Spin squeezing of atoms by the dipole interaction in virtually excited Rydberg states, *Phys. Rev. A* **65**, 041803(R) (2002).
- [22] J. E. Johnson and S. L. Rolston, Interactions between Rydberg-dressed atoms, *Phys. Rev. A* **82**, 033412 (2010).
- [23] N. Henkel, R. Nath, and T. Pohl, Three-dimensional roton excitations and supersolid formation in Rydberg-excited Bose-Einstein condensates, *Phys. Rev. Lett.* **104**, 195302 (2010).
- [24] G. Pupillo, A. Micheli, M. Boninsegni, I. Lesanovsky, and P. Zoller, Strongly correlated gases of Rydberg-dressed atoms: Quantum and classical dynamics, *Phys. Rev. Lett.* **104**, 223002 (2010).
- [25] J. Honer, H. Weimer, T. Pfau, and H. P. Büchler, Collective many-body interaction in Rydberg dressed atoms, *Phys. Rev. Lett.* **105**, 160404 (2010).
- [26] F. Grusdt and M. Fleischhauer, Fractional quantum Hall physics with ultracold Rydberg gases in artificial gauge fields, *Phys. Rev. A* **87**, 043628 (2013).
- [27] M. Mattioli, M. Dalmonte, W. Lechner, and G. Pupillo, Cluster Luttinger liquids of Rydberg-dressed atoms in optical lattices, *Phys. Rev. Lett.* **111**, 165302 (2013).
- [28] L. I. R. Gil, R. Mukherjee, E. M. Bridge, M. P. A. Jones, and T. Pohl, Spin squeezing in a Rydberg lattice clock, *Phys. Rev. Lett.* **112**, 103601 (2014).
- [29] A. W. Glaetzle, M. Dalmonte, R. Nath, I. Rousochatzakis, R. Moessner, and P. Zoller, Quantum spin-ice and Dimer models with Rydberg atoms, *Phys. Rev. X* **4**, 041037 (2014).
- [30] J. B. Balewski, A. T. Krupp, A. Gaj, S. Hofferberth, R. Löw, and T. Pfau, Rydberg dressing: Understanding of collective many-body effects and implications for experiments, *New J. Phys.* **16**, 063012 (2014).
- [31] R. M. W. van Bijnen and T. Pohl, Quantum magnetism and topological ordering via Rydberg dressing near Förster resonances, *Phys. Rev. Lett.* **114**, 243002 (2015).
- [32] X. Li and S. D. Sarma, Exotic topological density waves in cold atomic Rydberg-dressed fermions, *Nat. Commun.* **6**, 7137 (2015).
- [33] A. W. Glaetzle, M. Dalmonte, R. Nath, C. Gross, I. Bloch, and P. Zoller, Designing frustrated quantum magnets with laser-dressed Rydberg atoms, *Phys. Rev. Lett.* **114**, 173002 (2015).
- [34] A. W. Glaetzle, R. M. van Bijnen, P. Zoller, and W. Lechner, A coherent quantum annealer with Rydberg atoms, *Nat. Commun.* **8**, 15813 (2017).
- [35] I.-D. Potirniche, A. C. Potter, M. Schleier-Smith, A. Vishwanath, and N. Y. Yao, Floquet symmetry-protected topological phases in cold-atom systems, *Phys. Rev. Lett.* **119**, 123601 (2017).
- [36] R. Kaubruegger, P. Silvi, C. Kokail, R. van Bijnen, A. M. Rey, J. Ye, A. M. Kaufman, and P. Zoller, Variational spin-squeezing algorithms on programmable quantum sensors, *Phys. Rev. Lett.* **123**, 260505 (2019).
- [37] A. Mitra, M. J. Martin, G. W. Biedermann, A. M. Marino, P. M. Poggi, and I. H. Deutsch, Robust Mølmer-Sørensen gate for neutral atoms using rapid adiabatic Rydberg dressing, *Phys. Rev. A* **101**, 030301(R) (2020).
- [38] J. T. Young, S. R. Muleady, M. A. Perlin, A. M. Kaufman, and A. M. Rey, Enhancing spin squeezing using soft-core interactions, *Phys. Rev. Res.* **5**, L012033 (2023).
- [39] Y.-Y. Jau, A. Hankin, T. Keating, I. H. Deutsch, and G. Biedermann, Entangling atomic spins with a Rydberg-dressed spin-flip blockade, *Nat. Phys.* **12**, 71 (2016).
- [40] J. Zeiher, R. Van Bijnen, P. Schauß, S. Hild, J.-y. Choi, T. Pohl, I. Bloch, and C. Gross, Many-body interferometry of a Rydberg-dressed spin lattice, *Nat. Phys.* **12**, 1095 (2016).
- [41] J. Zeiher, J.-y. Choi, A. Rubio-Abadal, T. Pohl, R. van Bijnen, I. Bloch, and C. Gross, Coherent many-body spin dynamics in a long-range interacting Ising chain, *Phys. Rev. X* **7**, 041063 (2017).
- [42] V. Borish, O. Marković, J. A. Hines, S. V. Rajagopal, and M. Schleier-Smith, Transverse-field Ising dynamics in a Rydberg-dressed atomic gas, *Phys. Rev. Lett.* **124**, 063601 (2020).
- [43] L.-M. Steinert, P. Osterholz, R. Eberhard, L. Festa, N. Lorenz, Z. Chen, A. Trautmann, and C. Gross, Spatially tunable spin interactions in neutral atom arrays, *Phys. Rev. Lett.* **130**, 243001 (2023).
- [44] E. Guardado-Sanchez, B. M. Spar, P. Schauss, R. Belyansky, J. T. Young, P. Bienias, A. V. Gorshkov, T. Iadecola, and W. S. Bakr, Quench dynamics of a Fermi gas with strong nonlocal interactions, *Phys. Rev. X* **11**, 021036 (2021).
- [45] P. Weckesser, K. Srakaew, T. Blatz, D. Wei, D. Adler, S. Agrawal, A. Bohrdt, I. Bloch, and J. Zeiher, Realization of a Rydberg-dressed extended Bose Hubbard model, [arXiv: 2405.20128](https://arxiv.org/abs/2405.20128).

- [46] T. F. Gallagher and W. E. Cooke, Interactions of blackbody radiation with atoms, *Phys. Rev. Lett.* **42**, 835 (1979).
- [47] I. Mourachko, D. Comparat, F. de Tomasi, A. Fioretti, P. Nosbaum, V. M. Akulin, and P. Pillet, Many-body effects in a frozen Rydberg gas, *Phys. Rev. Lett.* **80**, 253 (1998).
- [48] W. R. Anderson, J. R. Veale, and T. F. Gallagher, Resonant dipole-dipole energy transfer in a nearly frozen Rydberg gas, *Phys. Rev. Lett.* **80**, 249 (1998).
- [49] L. Festa, N. Lorenz, L.-M. Steinert, Z. Chen, P. Osterholz, R. Eberhard, and C. Gross, Blackbody-radiation-induced facilitated excitation of Rydberg atoms in optical tweezers, *Phys. Rev. A* **105**, 013109 (2022).
- [50] S. Hollerith, K. Srakaew, D. Wei, A. Rubio-Abadal, D. Adler, P. Weckesser, A. Kruckenhauser, V. Walther, R. van Bijnen, J. Rui, C. Gross, I. Bloch, and J. Zeiher, Realizing distance-selective interactions in a Rydberg-dressed atom array, *Phys. Rev. Lett.* **128**, 113602 (2022).
- [51] E. A. Goldschmidt, T. Boulier, R. C. Brown, S. B. Koller, J. T. Young, A. V. Gorshkov, S. L. Rolston, and J. V. Porto, Anomalous broadening in driven dissipative Rydberg systems, *Phys. Rev. Lett.* **116**, 113001 (2016).
- [52] J. A. Aman, B. J. DeSalvo, F. B. Dunning, T. C. Killian, S. Yoshida, and J. Burgdörfer, Trap losses induced by near-resonant Rydberg dressing of cold atomic gases, *Phys. Rev. A* **93**, 043425 (2016).
- [53] T. Boulier, E. Magnan, C. Bracamontes, J. Maslek, E. A. Goldschmidt, J. T. Young, A. V. Gorshkov, S. L. Rolston, and J. V. Porto, Spontaneous avalanche dephasing in large Rydberg ensembles, *Phys. Rev. A* **96**, 053409 (2017).
- [54] See Supplemental Material at <http://link.aps.org/supplemental/10.1103/PhysRevLett.134.133201>, which includes Refs. [55–63], for details on the autoionization process and many-body effects in Rydberg dressing.
- [55] T. Ido, T. H. Loftus, M. M. Boyd, A. D. Ludlow, K. W. Holman, and J. Ye, Precision spectroscopy and density-dependent frequency shifts in ultracold Sr, *Phys. Rev. Lett.* **94**, 153001 (2005).
- [56] C. E. Moore, *Atomic Energy Levels*, Natl. Bur. Stand. Ref. Data Ser., Natl. Bur. Stand. (U.S.) Circ. No. 35 (U.S. GPO, Washington, DC, 1971), Vol. II.
- [57] C. Cohen-Tannoudji, J. Dupont-Roc, and G. Grynberg, *Atom-Photon Interactions: Basic Processes and Applications* (Wiley, New York, 1998).
- [58] L. Couturier, I. Nosske, F. Hu, C. Tan, C. Qiao, Y. H. Jiang, P. Chen, and M. Weidemüller, Measurement of the strontium triplet Rydberg series by depletion spectroscopy of ultracold atoms, *Phys. Rev. A* **99**, 022503 (2019).
- [59] A. Gallagher, Oscillator strengths of Ca II, Sr II, and Ba II, *Phys. Rev.* **157**, 24 (1967).
- [60] R. Grimm, M. Weidemüller, and Y. B. Ovchinnikov, Optical dipole traps for neutral atoms, *Adv. At. Mol. Opt. Phys.* **42**, 95 (2000).
- [61] M. Safronova (private communication).
- [62] N. Šibalić, J. Pritchard, C. Adams, and K. Weatherill, ARC: An open-source library for calculating properties of alkali Rydberg atoms, *Comput. Phys. Commun.* **220**, 319 (2017).
- [63] E. J. Robertson, N. Šibalić, R. M. Potvliege, and M. P. A. Jones, ARC 3.0: An expanded Python toolbox for atomic physics calculations, *Comput. Phys. Commun.* **261**, 107814 (2021).
- [64] J. Zeiher, Realization of Rydberg-dressed quantum magnets, Ph.D. thesis, Ludwig Maximilians Universität München, 2017.
- [65] Independent of the collective loss issue, a low duty cycle can offer fundamental benefits when bridging the gap between the Rydberg dressing interaction energy and a slower timescale such as tunneling in an optical lattice, as discussed and demonstrated in Ref. [45].
- [66] W. E. Cooke, T. F. Gallagher, S. A. Edelstein, and R. M. Hill, Doubly excited autoionizing Rydberg states of Sr, *Phys. Rev. Lett.* **40**, 178 (1978).
- [67] E. Y. Xu, Y. Zhu, O. C. Mullins, and T. F. Gallagher, Sr $5p_{1/2}ns_{1/2}$ and $5p_{3/2}ns_{1/2}$ $J = 1$ autoionizing states, *Phys. Rev. A* **33**, 2401 (1986).
- [68] J. Millen, G. Lochead, G. R. Corbett, R. M. Potvliege, and M. P. A. Jones, Spectroscopy of a cold strontium Rydberg gas, *J. Phys. B* **44**, 184001 (2011).
- [69] G. Lochead, D. Boddy, D. P. Sadler, C. S. Adams, and M. P. A. Jones, Number-resolved imaging of excited-state atoms using a scanning autoionization microscope, *Phys. Rev. A* **87**, 053409 (2013).
- [70] P. McQuillen, X. Zhang, T. Strickler, F. B. Dunning, and T. C. Killian, Imaging the evolution of an ultracold strontium Rydberg gas, *Phys. Rev. A* **87**, 013407 (2013).
- [71] I. S. Madjarov, J. P. Covey, A. L. Shaw, J. Choi, A. Kale, A. Cooper, H. Pichler, V. Schkolnik, J. R. Williams, and M. Endres, High-fidelity entanglement and detection of alkaline-earth Rydberg atoms, *Nat. Phys.* **16**, 857 (2020).
- [72] S. Ma, A. P. Burgers, G. Liu, J. Wilson, B. Zhang, and J. D. Thompson, Universal gate operations on nuclear spin qubits in an optical tweezer array of ^{171}Yb Atoms, *Phys. Rev. X* **12**, 021028 (2022).
- [73] A. P. Burgers, S. Ma, S. Saskin, J. Wilson, M. A. Alarcón, C. H. Greene, and J. D. Thompson, Controlling Rydberg excitations using ion-core transitions in alkaline-earth atom-tweezer arrays, *PRX Quantum* **3**, 020326 (2022).
- [74] K.-L. Pham, T. F. Gallagher, P. Pillet, S. Lepoutre, and P. Cheinet, Coherent light shift on alkaline-earth Rydberg atoms from isolated core excitation without autoionization, *PRX Quantum* **3**, 020327 (2022).
- [75] R. Mukherjee, J. Millen, R. Nath, M. P. A. Jones, and T. Pohl, Many-body physics with alkaline-earth Rydberg lattices, *J. Phys. B* **44**, 184010 (2011).
- [76] W. E. Cooke and T. F. Gallagher, Calculation of autoionization rates for high-angular-momentum Rydberg states, *Phys. Rev. A* **19**, 2151 (1979).
- [77] S. Yoshida, J. Burgdörfer, R. Brienza, G. Fields, and F. B. Dunning, $5p_{1/2}n\ell_j$ autoionizing states of strontium for $0 \leq \ell \leq 5$, *Phys. Rev. A* **107**, 043112 (2023).
- [78] The electron ejected by the AI departs rapidly due to its drastically smaller mass. The mass ratio between a $^{88}\text{Sr}^+$ ion and an electron is of order 10^5 , and the departure time under constant acceleration scales inversely with the square root of the mass.
- [79] H. Levine, A. Keesling, A. Omran, H. Bernien, S. Schwartz, A. S. Zibrov, M. Endres, M. Greiner, V. Vuletić, and M. D. Lukin, High-fidelity control and entanglement of Rydberg-atom qubits, *Phys. Rev. Lett.* **121**, 123603 (2018).
- [80] J. T. Young, T. Boulier, E. Magnan, E. A. Goldschmidt, R. M. Wilson, S. L. Rolston, J. V. Porto, and A. V.

- Gorshkov, Dissipation-induced dipole blockade and anti-blockade in driven Rydberg systems, *Phys. Rev. A* **97**, 023424 (2018).
- [81] D.J. Wineland, J.J. Bollinger, W.M. Itano, F.L. Moore, and D.J. Heinzen, Spin squeezing and reduced quantum noise in spectroscopy, *Phys. Rev. A* **46**, R6797 (1992).
- [82] D.J. Wineland, J.J. Bollinger, W.M. Itano, and D.J. Heinzen, Squeezed atomic states and projection noise in spectroscopy, *Phys. Rev. A* **50**, 67 (1994).
- [83] M. Kitagawa and M. Ueda, Squeezed spin states, *Phys. Rev. A* **47**, 5138 (1993).
- [84] R. Loew, U. Raitzsch, R. Heidemann, V. Bendkowsky, B. Butscher, A. Grabowski, and T. Pfau, Apparatus for excitation and detection of Rydberg atoms in quantum gases, [arXiv:0706.2639](https://arxiv.org/abs/0706.2639).
- [85] Y. Wu, S. Kolkowitz, S. Puri, and J. D. Thompson, Erasure conversion for fault-tolerant quantum computing in alkaline earth Rydberg atom arrays, *Nat. Commun.* **13**, 4657 (2022).